



## Article

# Regulating Al<sub>2</sub>O<sub>3</sub>/PAN/PEG Nanofiber Membranes with Suitable Phase Change Thermoregulation Features

Leping Huang <sup>1</sup>, Ying Chen <sup>1</sup>, Zhaobao Xu <sup>2</sup>, Cui He <sup>2</sup>, Youmu Li <sup>1</sup>, Jinchao Zhao <sup>2,\*</sup>  and Youhong Tang <sup>3,\*</sup> 

- <sup>1</sup> College of Materials Science and Engineering, Wuhan Textile University, Wuhan 430200, China; lphuang@wtu.edu.cn (L.H.); 2215043051@mail.wtu.edu.cn (Y.C.); 2215383110@mail.wtu.edu.cn (Y.L.)
- <sup>2</sup> Hubei Provincial Engineering Laboratory for Clean Production and High Value Utilization of Bio-Based Textile Materials, Wuhan Textile University, Wuhan 430200, China; zhaobao.xu@lianhetech.com (Z.X.); hecui10127@outlook.com (C.H.)
- <sup>3</sup> Flinders Institute for NanoScale Science and Technology, College of Science and Engineering, Flinders University, Adelaide, SA 5042, Australia
- \* Correspondence: jczhao@wtu.edu.cn (J.Z.); youhong.tang@flinders.edu.au (Y.T.)

**Abstract:** To address the thermal comfort needs of the human body, the development of personal thermal management textile is critical. Phase change materials (PCMs) have a wide range of applications in thermal management due to their large thermal storage capacity and their isothermal properties during phase change. However, their inherent low thermal conductivity and susceptibility to leakage severely limit their application range. In this study, polyethylene glycol (PEG) was used as the PCM and polyacrylonitrile (PAN) as the polymer backbone, and the thermal conductivity was increased by adding spherical nano-alumina (Al<sub>2</sub>O<sub>3</sub>). Utilizing coaxial electrospinning technology, phase-change thermoregulated nanofiber membranes with a core-shell structure were created. The study demonstrates that the membranes perform best in terms of thermal responsiveness and thermoregulation when 5% Al<sub>2</sub>O<sub>3</sub> is added. The prepared nanofiber membranes have a melting enthalpy of 60.05 J·g<sup>-1</sup> and retain a high enthalpy after 50 cycles of cold and heat, thus withstanding sudden changes in ambient temperature well. Additionally, the nanofiber membranes have excellent air permeability and high moisture permeability, which can increase wearer comfort. As a result, the constructed coaxial phase change thermoregulated nanofiber membranes can be used as a promising textile for personal thermal management.

**Keywords:** coaxial electrospinning; nanofiber membranes; core-shell structure; phase change; temperature-regulating



**Citation:** Huang, L.; Chen, Y.; Xu, Z.; He, C.; Li, Y.; Zhao, J.; Tang, Y. Regulating Al<sub>2</sub>O<sub>3</sub>/PAN/PEG Nanofiber Membranes with Suitable Phase Change Thermoregulation Features. *Nanomaterials* **2023**, *13*, 2313. <https://doi.org/10.3390/nano13162313>

Academic Editor: Nicole Demarquette

Received: 12 July 2023

Revised: 7 August 2023

Accepted: 10 August 2023

Published: 12 August 2023



**Copyright:** © 2023 by the authors. Licensee MDPI, Basel, Switzerland. This article is an open access article distributed under the terms and conditions of the Creative Commons Attribution (CC BY) license (<https://creativecommons.org/licenses/by/4.0/>).

## 1. Introduction

The state of one's health can be impacted by thermal comfort. By protecting the body from the outside elements and insulating the air from the human body, clothing is essential to ensuring that the body's internal temperature remains consistent [1–4]. Through two major principles, advanced textiles for personal thermal management (PTM) are intended to increase body heat production and decrease heat loss from the body. In reaction to changes in the external environment and the body's internal temperature, these intelligent thermoregulation textiles may actively regulate the temperature of the microenvironment within the body, improving human comfort [5–9]. It is more accurate and energy efficient than traditional indoor thermal regulation methods.

Phase change materials (PCMs) are substances that absorb or release heat from the environment through their phase change within a specific temperature range [10–12]. PCMs have the capacity to swiftly absorb, diffuse, and release heat, enabling bi-directional temperature regulation [13–18]. PCM-based textiles exhibit a cushioning effect on the environment and can keep the body in a comfortable temperature range [19–23]. Polyethylene glycol (PEG) is a typical polymeric PCM. PEGs of various molecular weights can be combined

by heating to the necessary phase transition temperature to satisfy the body's comfort requirements. PEG plays a significant role in temperature-regulating textiles because it has the properties of structural rule, strong crystallinity, good biocompatibility, and high latent heat of phase change.

However, PCM in mixed fibers can be easily removed through cleaning, wiping, or abrasion, and there is also the issue of leaking during the phase change process, which results in poor material stability and a short service life [24–26]. To tackle this challenge, encapsulation technology for PCM has become the focus of the study. Container packaging, microencapsulation, porous adsorption, electrostatic spinning, and other technologies are commonly used for encapsulation [27–29]. Electrostatic spinning is a simple and effective new technology for processing micro and nanofibers that has a wide range of applications in biomedical materials, filtration protection, catalysis, energy, optoelectronics, food engineering, cosmetics, and other areas. It has the benefits of variable fiber composition, fine customizable structure, big specific surface area, high porosity, and good flexibility of the manufactured fibers, which may suit human comfort requirements [30–32]. Coaxial electrospinning has shown its obvious advantages, with concentrically arranged spinnerets connected to separate channels of different solutions allowing the direct production of fibers with a core-shell structure. PEG can be directly encapsulated in the core layer of the polymer using coaxial electrospinning to solve leakage problems [33,34]. PEG has the disadvantage of poor thermal conductivity, which limits its heat transfer properties [35]. However, the thermal conductivity of PCM is important, as this determines the rate at which the PCM reaches the solid-liquid transition and also affects the efficiency of energy storage and release [36,37]. This problem can be solved by adding nanoscale thermally conductive fillers such as graphene, copper particles, alumina, etc. Among them, nano-alumina has excellent properties like high thermal conductivity, good insulation, great hardness, high-temperature resistance, corrosion resistance, wear resistance, excellent flowability, and controllable particle size distribution. In this study, spherical nano-alumina ( $\text{Al}_2\text{O}_3$ ) is added to PCM based on PEG to improve the thermal conductivity of PCM. High latent heat, fast heat transfer, good circulation stability, and the ability to meet human comfort needs are the directions for the development of phase change thermoregulated textiles. To fulfill the needs of the human body, we combined PEGs with different molecular weights and regulated their phase change temperatures to the range of 33–38 °C. The composite PEG was then used as the core layer, polyacrylonitrile (PAN) was used as the shell layer, and  $\text{Al}_2\text{O}_3$  was added to the shell layer to prepare the core-shell structure of  $\text{Al}_2\text{O}_3$ /PAN/PEG phase change thermoregulation nanofiber membranes. The results show that the nanofiber membranes prepared in this research are promising for PTM.

## 2. Materials and Methods

### 2.1. Materials

Polyacrylonitrile (PAN, average Mw = 150,000) was purchased from Shanghai Macklin Biochemical Technology Co., Ltd., China. N, N-dimethylformamide (DMF) and PEG1500 were purchased from Sinopharm Group Co., Ltd., Shanghai, China. PEG1000 was purchased from Xi'an Tianzheng Co., Ltd., China. Spherical nano-alumina ( $\text{Al}_2\text{O}_3$ , average particle size of 30 nm) was purchased from Beijing Deke Daojin Science and Pharmaceutical Technology Co., Ltd., China. All these materials were used without further processing and purification.

### 2.2. Compounding of PEG

The phase-change temperature of pure PEG with different molecular weights was characterized by a differential scanning thermal analyzer (DSC, 200F3, NETZSCH, Selb, Germany), and then the optimal mixture ratio was determined by using the Schröder Equation (1):

$$T = \frac{1}{\frac{1}{T_f} - \frac{R \ln X_A}{\Delta_s H_A}} \quad (1)$$

where  $X_A$  is the mole fraction of pure solid compound  $A$  in the composite phase change material,  $\Delta_s^l H_A$  is the phase change enthalpy of pure solid compound  $A$ ,  $T_f$  is the phase change temperature of pure solid compound  $A$ ,  $T$  is the phase change temperature of the composite PCM containing solid compound  $A$ , and  $R$  is the gas constant. A hot melting process was used to combine PEG with different molecular weights at the theoretical ideal ratio. The DSC test confirmed the theoretical ratio's rationality. The composite PEG with a phase change temperature of 33–38 °C was chosen as the core spinning solution.

### 2.3. Preparation of Shell-Spinning Solution

A certain mass of  $\text{Al}_2\text{O}_3$  was dispersed in DMF and sonicated for 1 h. Then, PAN was added and agitated for 2 h at a constant temperature of 70 °C to generate an  $\text{Al}_2\text{O}_3$ /PAN shell-spinning solution containing 10% PAN. In the experiment, the concentrations of regulated  $\text{Al}_2\text{O}_3$  were 1%, 3%, 5%, 7%, and 9%, respectively.

### 2.4. Preparation of $\text{Al}_2\text{O}_3$ /PAN/PEG Nanofiber Membranes

The prepared solution was transferred into a 20 mL disposable syringe, and electrostatic spinning was performed with a coaxial needle with an inner diameter of 20 G and an outer diameter of 14 G. Electrostatic spinning was performed at an applied voltage of 16 kV, a spinning distance of 10 cm, a core layer advancement speed of  $0.015 \text{ mm}\cdot\text{min}^{-1}$ , a shell layer advancement speed of  $0.08 \text{ mm}\cdot\text{min}^{-1}$ , and a drum receiver speed of  $100 \text{ r}\cdot\text{min}^{-1}$  for 2 h. Finally, the obtained nanofiber membranes were vacuum dried at room temperature for 24 h and stored in a desiccator for use. According to the change of  $\text{Al}_2\text{O}_3$  concentration, the resulting phase change thermoregulation nanofiber membranes were named 1%  $\text{Al}_2\text{O}_3$ /PAN/PEG, 3%  $\text{Al}_2\text{O}_3$ /PAN/PEG, 5%  $\text{Al}_2\text{O}_3$ /PAN/PEG, 7%  $\text{Al}_2\text{O}_3$ /PAN/PEG, and 9%  $\text{Al}_2\text{O}_3$ /PAN/PEG, respectively. The schematic illustrations are shown in Figure 1.

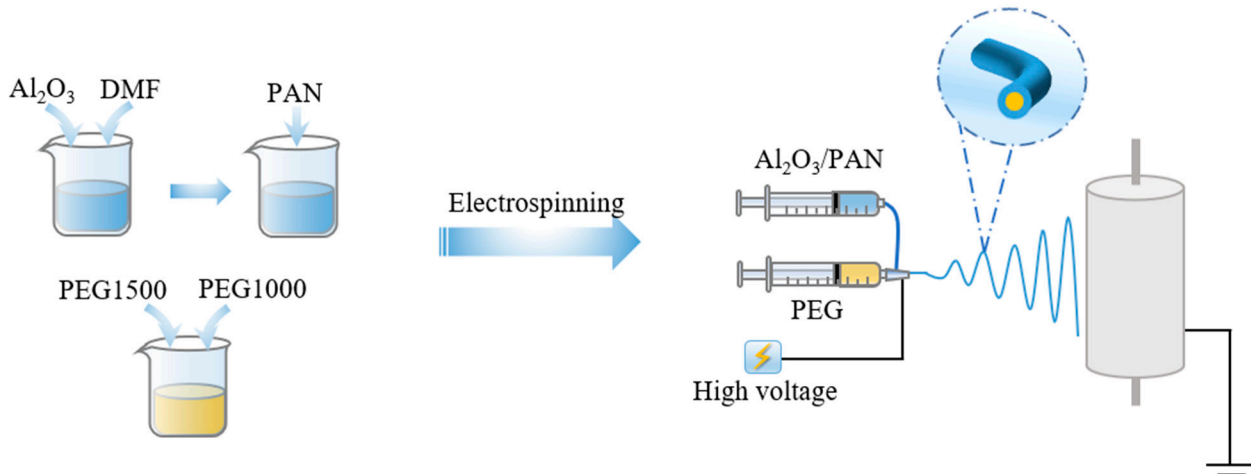


**Figure 1.** Schematic diagram of the preparation of phase change thermoregulated nanofiber membranes by coaxial electrospinning.

### 2.5. Characterization of $\text{Al}_2\text{O}_3$ /PAN/PEG Nanofiber Membranes

The surface morphology and structure features were determined using scanning electron microscopy (SEM, JSM-IT300, JEOL, Akishima, Japan). The thermal stability of the phase change nanofiber membranes were characterized by thermogravimetric analysis (STA 2500 Regulus, NETZSCH, Germany) with  $\text{N}_2$  as the protective gas, the temperature range of 30–800 °C, and the ramp-up rate of  $10 \text{ }^\circ\text{C}\cdot\text{min}^{-1}$ . The phase change behavior of the compounded PCMs and the phase change nanofiber membranes were characterized by differential scanning calorimetry (DSC, 200F3, NETZSCH, Selb, Germany) with  $\text{N}_2$  as the protective gas, the temperature range of 0–100 °C, and the ramp-up/down rate of  $10 \text{ }^\circ\text{C}\cdot\text{min}^{-1}$ . The membrane thermal regulating properties of the phase change nanofiber membranes

were characterized using infrared thermography (FLIR, E8, TELEDYNE, Boston, MA, USA) with a sample size of 2 cm × 2 cm × 0.01 cm, and the temperature of the hot bench was increased from room temperature to 50 °C. The air permeability of the phase change nanofiber membranes were characterized by a fabric air permeability tester (YG(B) 461G, Wenzhou Da Rong Spinning Instrument, Wenzhou, China). The moisture permeability of the phase change nanofiber membranes was tested by the evaporation method using a computerized fabric moisture meter (YG601H, Ningbo Textile Instrument Factory, Ningbo, China) at 38 °C, humidity of 50%, and gas flow rate of 0.3 m·s<sup>-1</sup>. The sample is weighed after being balanced for 0.5 h in the test chamber and then weighed again after 1 h of testing. The water vapor transmission rate (WVTR) is calculated according to Formula (2):

$$WVTR = \frac{W_1 - W_2}{S} \times 24 \quad (2)$$

where  $S$  is the effective test area (where  $S$  is  $2.826 \times 10^{-3}$  m<sup>2</sup>),  $W_1$  is the first weighing weight, and  $W_2$  is the second weighing weight [38].

### 3. Results and Discussion

#### 3.1. Ratio of Complex PEG

From the standpoint of the actual thermal management application, the phase transition behavior is of utmost significance. The DSC test results for PEG1500 and PEG1000's phase change temperature and thermal energy storage capacity are depicted in Figure 2a. The actual phase change temperature of PEG1500 and PEG1000 are 45.1 °C and 27.3 °C, respectively. The phase change enthalpy for PEG1500 and PEG1000 are 192.6 J·g<sup>-1</sup> and 154.3 J·g<sup>-1</sup>. The phase change temperatures of both materials do not meet the human comfort requirements. According to the Schröder equation, the theoretical phase change temperature of the composite PEG is 35 °C when the molar fraction ratio of PEG1500 to PEG1000 is 1:9 (i.e., 1:6 by mass). After DSC testing, the phase change temperature of the aforesaid blended PEG is 36.4 °C, and the phase change enthalpy is 170.1 J·g<sup>-1</sup>, which meets the human comfort requirements, as shown in Figure 2b. Therefore, PEG1500:PEG1000 = 1:9 was used as the core layer solution to prepare the phase change thermoregulated nanofiber membranes.

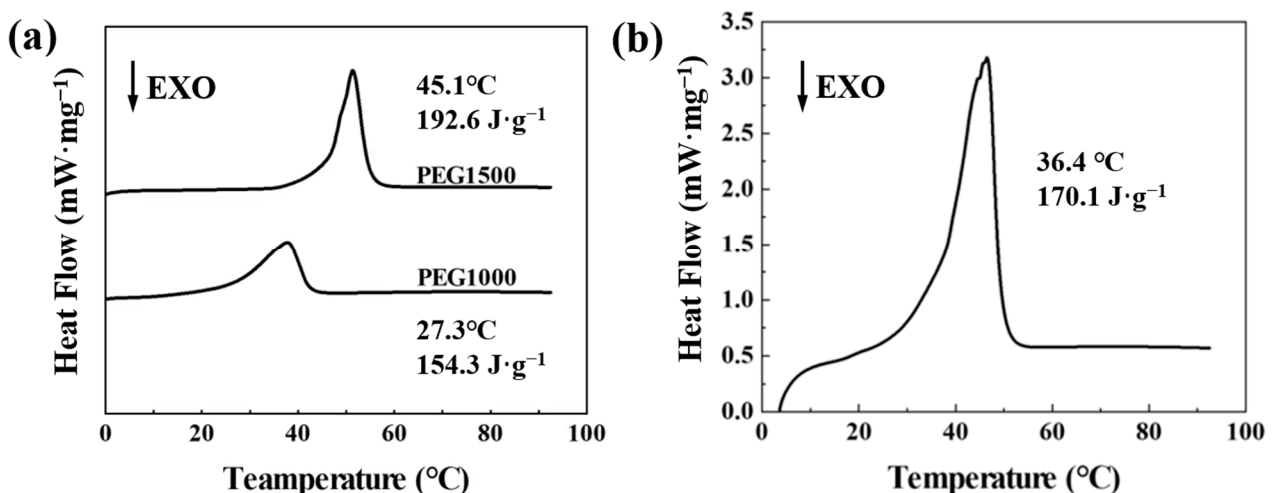


Figure 2. (a) DSC curves for PEG1500 and PEG1000. (b) DSC curve for PEG compounded at a 1:9 molar ratio of PEG1500 and PEG1000.

#### 3.2. The Structure and Morphology of Al<sub>2</sub>O<sub>3</sub>/PAN/PEG

To ensure that the PCM can be used properly above the melting point and does not leak, we have prepared phase change nanofiber membranes with a core-shell structure by encapsulating PEG in the fibers using coaxial electrospinning technology. Figure 3a–f



displays SEM images of nanofiber membranes prepared by adding  $\text{Al}_2\text{O}_3$  at 0%, 1%, 3%, 5%, 7%, and 9% concentrations to the shell layer, respectively. Randomly oriented cylindrical fibers can be observed.

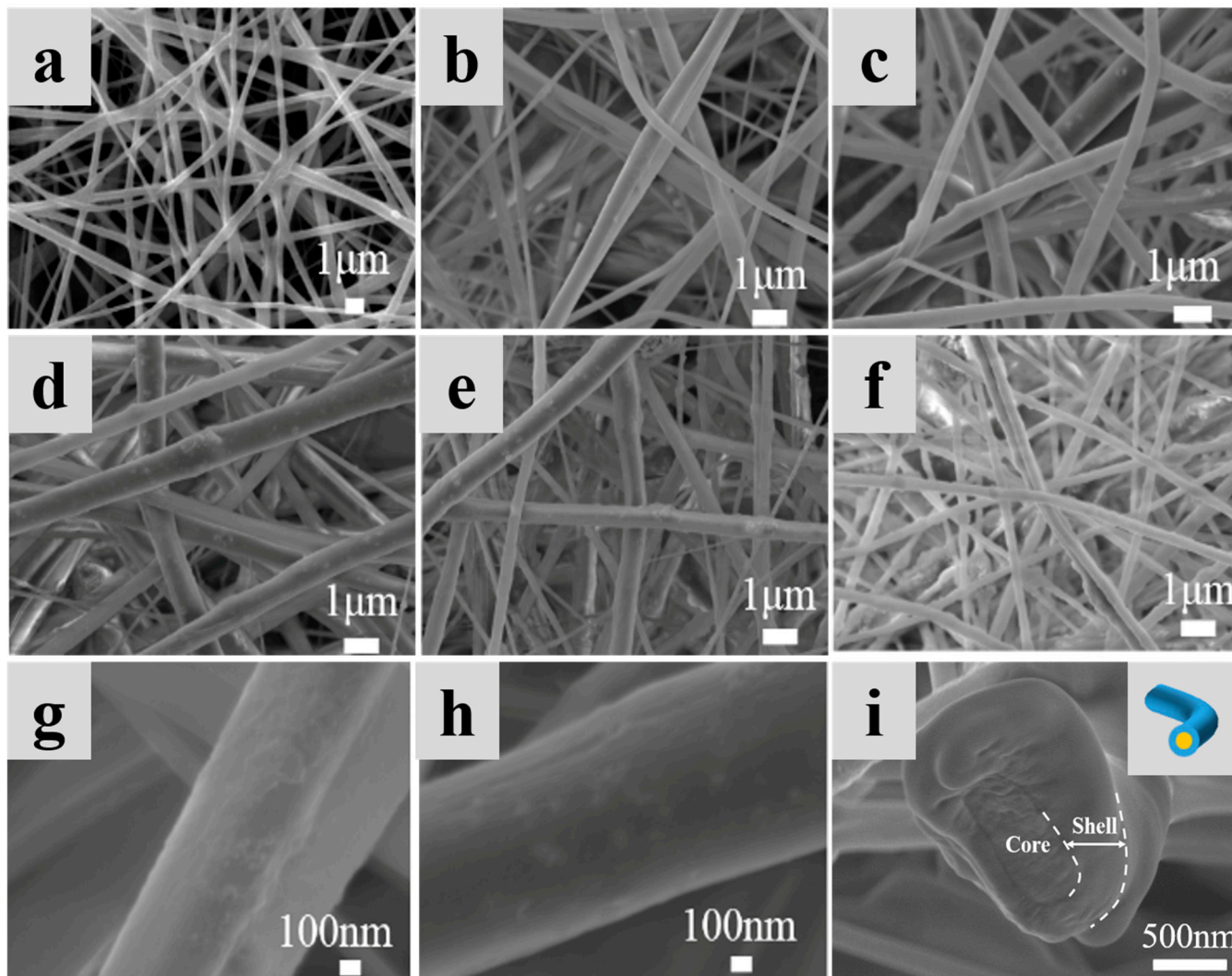


**Figure 3.** SEM images of nanofiber membranes containing different concentrations of  $\text{Al}_2\text{O}_3$ : (a) PAN/PEG, (b) 1%  $\text{Al}_2\text{O}_3$ /PAN/PEG, (c) 3%  $\text{Al}_2\text{O}_3$ /PAN/PEG, (d) 5%  $\text{Al}_2\text{O}_3$ /PAN/PEG, (e) 7%  $\text{Al}_2\text{O}_3$ /PAN/PEG and (f) 9%  $\text{Al}_2\text{O}_3$ /PAN/PEG. (g,h) are high-magnification images of (b,d), respectively. (i) is a cross-sectional view of 5%  $\text{Al}_2\text{O}_3$ /PAN/PEG, and the inset is a schematic diagram of a core-shell structured nanofiber.

The PAN/PEG fibers modified without the addition of  $\text{Al}_2\text{O}_3$  have the smallest diameter. As the concentration of  $\text{Al}_2\text{O}_3$  increases, it can be observed that the surface of the fibers gradually becomes rougher, the fibers become progressively thicker, and the diameter distribution becomes wider. The fibers are thickest when 5%  $\text{Al}_2\text{O}_3$  is added, with an average diameter of  $528 \pm 175$  nm. This was due to the increase in surface loading of the fibers as a result of the increase in  $\text{Al}_2\text{O}_3$  concentration in the shell layer. As the concentration of  $\text{Al}_2\text{O}_3$  continues to increase, the average diameter of the fibers gradually decreases, indicating that the amount of  $\text{Al}_2\text{O}_3$  loaded on the fiber surface has reached saturation. At the same time, the addition of  $\text{Al}_2\text{O}_3$  increases the viscosity of the spinning solution. The greater the viscosity, the more difficult it is to stretch the fibers under the electric field forces, the more difficult electrostatic spinning will be, and the larger the diameter of the fibers will be. In addition, the increased electrical conductivity of the spinning

solution enhances the stretching effect of the jet, leading to a reduction in the diameter of the fibers [39]. Based on SEM images, the diameter of the fibers and the variation of the fibers can be quantitatively assessed. The direct distribution of the various nanofiber membranes is shown in Figure 4, and the average diameter is shown in Table 1. The phenomenon of fibers adhering to each other can also be observed, which is caused by incomplete evaporation of the solvent from adjacent fibers. Figure 3g,h shows that as the  $\text{Al}_2\text{O}_3$  concentration increases from 0% to 5%, the distribution of  $\text{Al}_2\text{O}_3$  on the fiber surface increases and becomes more homogeneous. The higher the percentage of  $\text{Al}_2\text{O}_3$  in the fiber, the better the thermal conductivity. Figure 3i shows a cross-sectional view of the 5%  $\text{Al}_2\text{O}_3$ /PAN/PEG fiber, where a distinct core-shell structure can be observed, indicating that the addition of  $\text{Al}_2\text{O}_3$  barely affects the construction of the core-shell structure in the fiber and that the PEG well encapsulated.

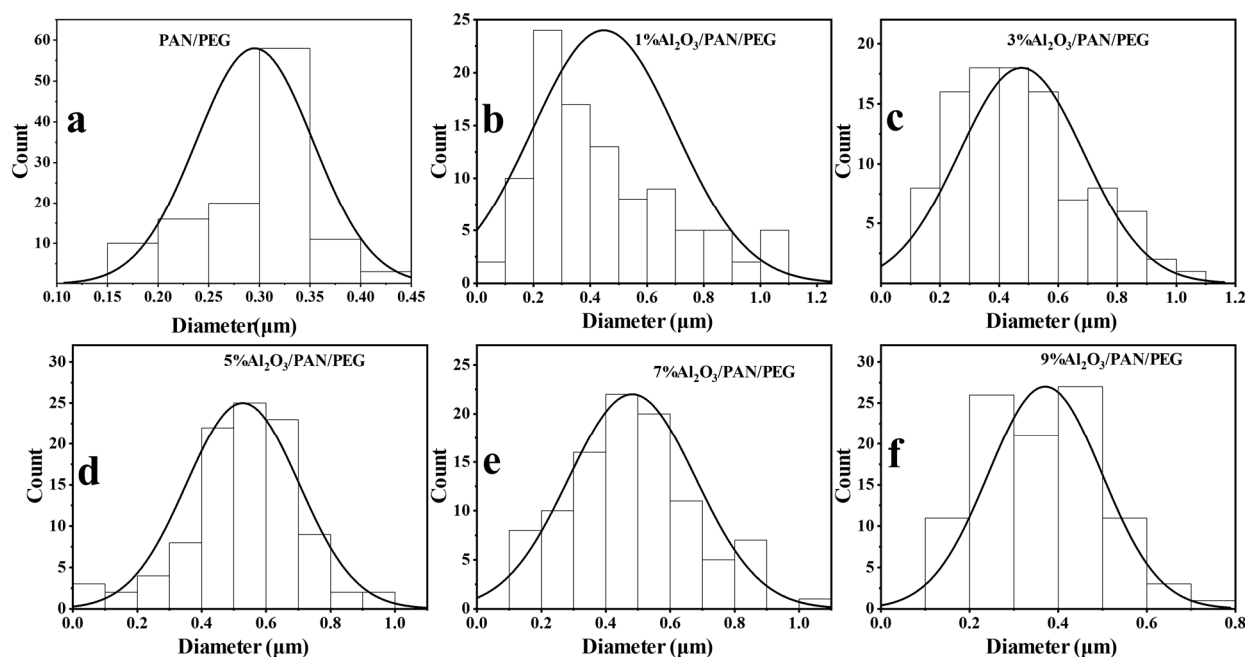


**Figure 4.** Distribution of diameters of nanofiber membranes containing different concentrations of  $\text{Al}_2\text{O}_3$ : (a) PAN/PEG, (b) 1%  $\text{Al}_2\text{O}_3$ /PAN/PEG, (c) 3%  $\text{Al}_2\text{O}_3$ /PAN/PEG, (d) 5%  $\text{Al}_2\text{O}_3$ /PAN/PEG, (e) 7%  $\text{Al}_2\text{O}_3$ /PAN/PEG, and (f) 9%  $\text{Al}_2\text{O}_3$ /PAN/PEG.

**Table 1.** Nanofiber diameter data for different  $\text{Al}_2\text{O}_3$  concentrations.

Sample	Average Diameter/nm	Standard Deviation/nm
PAN/PEG	300	150
1% $\text{Al}_2\text{O}_3$ /PAN/PEG	448	253
3% $\text{Al}_2\text{O}_3$ /PAN/PEG	476	211
5% $\text{Al}_2\text{O}_3$ /PAN/PEG	528	175
7% $\text{Al}_2\text{O}_3$ /PAN/PEG	482	197
9% $\text{Al}_2\text{O}_3$ /PAN/PEG	371	128

### 3.3. Thermal Stability Analysis

An important factor affecting the working temperature range of composites is the thermal stability of the material. To investigate the effect of  $\text{Al}_2\text{O}_3$  modification on the thermal stability of nanofiber membranes, thermogravimetric analysis was carried out on  $\text{Al}_2\text{O}_3$ , PAN, PAN/PEG, and 5%  $\text{Al}_2\text{O}_3$ /PAN/PEG. Figure 5 shows the TG and DTG curves, respectively. The thermogravimetric analysis shows that the degradation trends of  $\text{Al}_2\text{O}_3$ /PAN/PEG and PAN/PEG are similar. A two-step weight loss process occurs during

the warming process. At 300 °C, the weight loss components are dominated by PAN and water. The rate of degradation is greatest between 350 °C and 450 °C, with the main weight loss being the PEG fraction. At 50% weight loss, PAN is at 550 °C, while PAN/PEG and Al<sub>2</sub>O<sub>3</sub>/PAN/PEG are at 410 °C, indicating that PAN/PEG and Al<sub>2</sub>O<sub>3</sub>/PAN/PEG have better thermal stability than PAN. The decomposition temperature of Al<sub>2</sub>O<sub>3</sub>/PAN/PEG is 324 °C. After 550 °C, the curves are largely stable. The addition of Al<sub>2</sub>O<sub>3</sub> increased the residue from 24% to 31% compared to PAN/PEG after curves stabilization. These phenomena suggest that highly stable layers of Al<sub>2</sub>O<sub>3</sub> nanoparticles are involved in the carbon formation process, resulting in a denser and more stable carbon layer that boosts the internal matrix's resistance to thermal degradation.

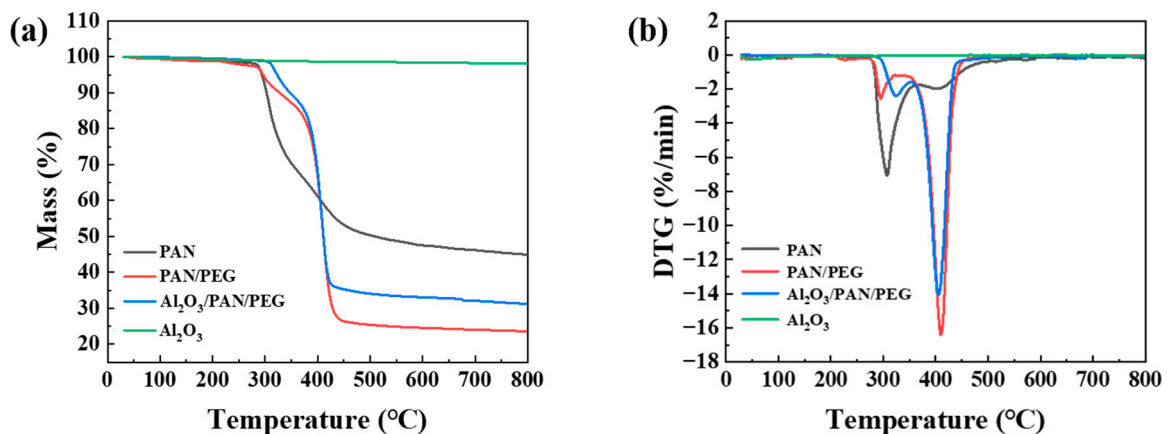
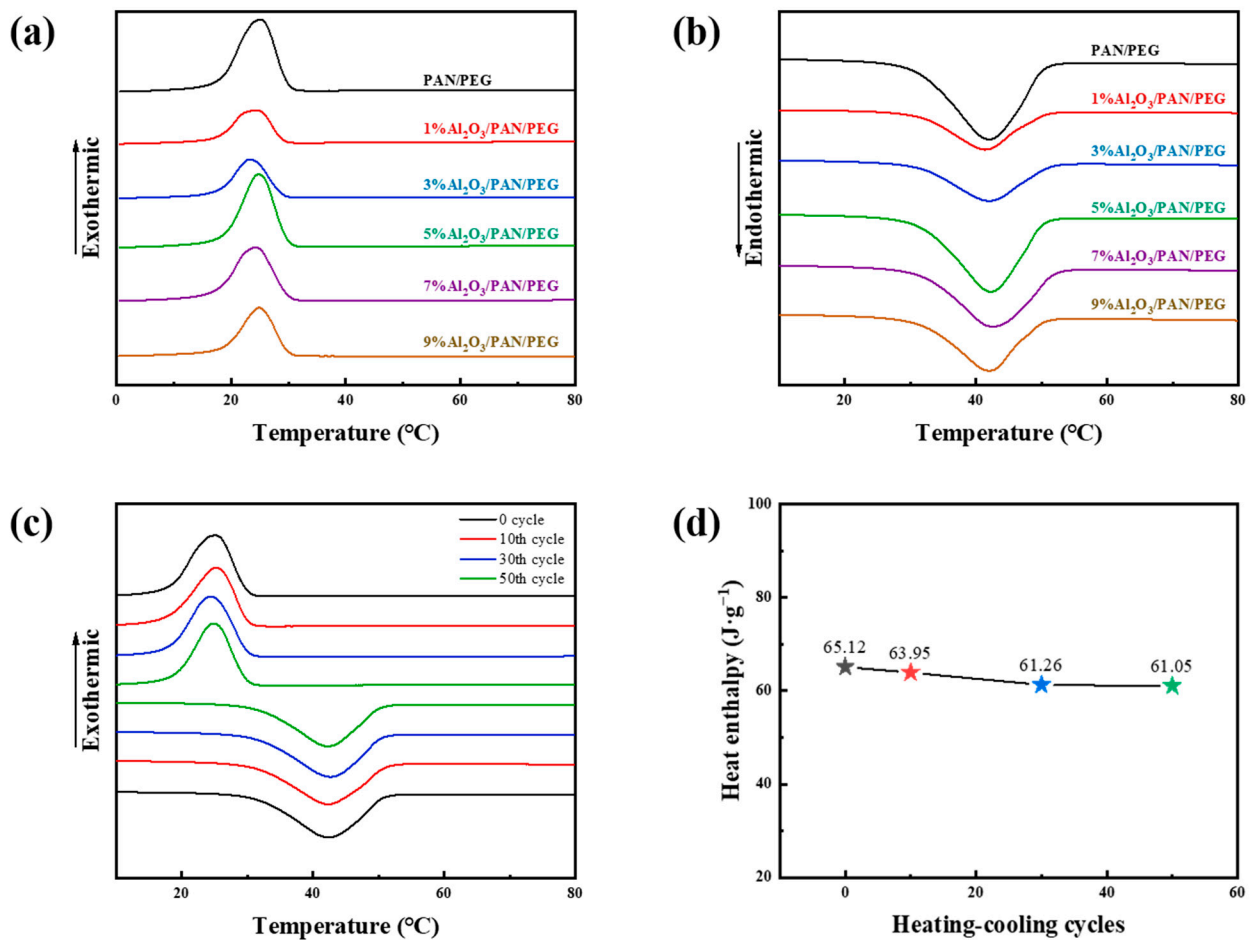


Figure 5. TG/DTG test diagram of PAN, PAN/PEG, 5% Al<sub>2</sub>O<sub>3</sub>/PAN/PEG: (a) TG and (b) DTG.

### 3.4. Analysis of Thermal Conductivity and Storage Performance

The latent heat properties of PCMs are important for assessing their thermal storage capacity. The phase transition temperature and thermal storage capacity of phase change nanofiber membranes with different Al<sub>2</sub>O<sub>3</sub> concentrations were investigated by differential scanning calorimetry. As shown in Figure 6, nanofiber membranes with different Al<sub>2</sub>O<sub>3</sub> concentrations exhibit similar characteristic profiles during heating and cooling, with both heat absorption and exothermic peaks, which are attributed to the reversible phase change. The exothermic peak is caused by nucleation crystallization, indicating a liquid–solid phase transition. The heat absorption peak corresponds to a phase change from an ordered crystalline phase to a disordered amorphous state and represents a solid–liquid phase transition. The latent heats of melting and cooling represent the energy released and absorbed during the heating and cooling processes and can visualize the ability of the PCM to thermally regulate in both directions. The DSC curves for these phase change nanofiber membranes all exhibit appropriate enthalpies and melting/cooling temperatures in the human comfort temperature range.



**Figure 6.** DSC curves of fibrous membranes with varying Al<sub>2</sub>O<sub>3</sub> concentrations during the (a) cooling and (b) melting processes. 5% Al<sub>2</sub>O<sub>3</sub>/PAN/PEG after heating and cooling cycles (c) DSC curves and (d) encapsulation efficiency plot.

As shown in Table 2, the melting point ( $T_m$ ) of PAN/PEG was 31.8 °C, close to human skin temperature, and the melting enthalpy ( $\Delta H_m$ ) of PAN/PEG was 70.38 J·g<sup>-1</sup>. However, the phase change nanofiber membranes prepared with the addition of Al<sub>2</sub>O<sub>3</sub> had lower enthalpy of melting and cooling compared to PAN/PEG due to the fact that only PEG was responsible for the composite fiber in a certain temperature range. The introduction of Al<sub>2</sub>O<sub>3</sub> reduces the mass ratio of PEG. In addition, PEG has the disadvantage of being poorly spinnable, which affects the amount of PEG encapsulated in the fiber, while increasing the PEG content helps to enhance the latent heat of phase change of the PCM. It is worth noting that the peak melt temperature ( $T_{mp}$ ) shifts towards a lower temperature with the addition of Al<sub>2</sub>O<sub>3</sub>. This is because the Al<sub>2</sub>O<sub>3</sub> addition makes the fibrous membrane more thermally sensitive, which makes it simpler for the PEG to reach the phase change. After modification with Al<sub>2</sub>O<sub>3</sub>, the enthalpy of 5% Al<sub>2</sub>O<sub>3</sub>/PAN/PEG is the highest at 60.05 J·g<sup>-1</sup>. The thickest fiber and saturation of the surface Al<sub>2</sub>O<sub>3</sub> at this point are consistent with the morphological analysis above. Compared to PAN/PEG, the cooling enthalpy ( $\Delta H_c$ ) for 5% Al<sub>2</sub>O<sub>3</sub>/PAN/PEG is lower, and the onset of cooling temperature ( $T_{co}$ ) is slightly higher. These are most likely owing to the inclusion of Al<sub>2</sub>O<sub>3</sub>, which improves heat transfer and results in a lower nucleation barrier for the PEG to form stable nuclei, hence boosting cooling temperature and decreasing cooling enthalpy. In summary, 5% Al<sub>2</sub>O<sub>3</sub>/PAN/PEG has high latent heat and thermal sensitivity. Furthermore, because of the appropriate  $T_m$ , this material is a practical candidate for thermally regulated textiles.



**Table 2.** Enthalpy of nanofiber membranes with different Al<sub>2</sub>O<sub>3</sub> concentrations.

Sample	Melting			Cooling		
	$T_{mo}/^{\circ}\text{C}$	$T_{mp}/^{\circ}\text{C}$	$\Delta H_m/\text{J}\cdot\text{g}^{-1}$	$T_{co}/^{\circ}\text{C}$	$T_{cp}/^{\circ}\text{C}$	$\Delta H_c/\text{J}\cdot\text{g}^{-1}$
PAN/PEG	31.8	42.3	70.38	18.4	25.1	−69.12
1%Al <sub>2</sub> O <sub>3</sub> /PAN/PEG	31.5	41.4	30.48	18.0	24.6	−27.64
3%Al <sub>2</sub> O <sub>3</sub> /PAN/PEG	31.6	41.3	32.62	18.2	23.3	−30.36
5%Al <sub>2</sub> O <sub>3</sub> /PAN/PEG	31.9	41.1	60.05	19.1	24.8	−54.78
7%Al <sub>2</sub> O <sub>3</sub> /PAN/PEG	32.3	41.2	52.01	18.0	24.3	−47.06
9%Al <sub>2</sub> O <sub>3</sub> /PAN/PEG	32.2	41.6	41.34	19.2	25.0	−36.39

Note:  $T_m$  is the melt temperature on the ramp-up scan curve;  $T_{mo}$  is the melt onset temperature;  $T_{mp}$  is the peak melt temperature;  $\Delta H_m$  is the melting enthalpy;  $T_c$  is the cooling temperature on the ramp-down curve;  $T_{co}$  is the cooling onset temperature;  $T_{cp}$  is the peak cooling temperature; and  $\Delta H_c$  is the cooling enthalpy.

As the temperature rises, the phase change material transforms from a solid to a liquid. In the actual application process, the phase change material transformed into a liquid state is easy to flow in the core layer, and multiple cycles of melting and solidifying will also cause the flow of phase change material in the core layer. If the phase change material is not fully coated, it will easily leak out from it and be lost in the process of use due to friction, washing, and other factors, thus affecting its subsequent thermoregulation performance. The thermal cycling incalculability of phase change nanofiber membranes affects the effectiveness and lifetime of the material. To investigate the encapsulation stability of phase change nanofiber membranes, heating/cooling cycles of 5% Al<sub>2</sub>O<sub>3</sub>/PAN/PEG were carried out in a constant temperature oven at 20 to 70 °C. The phase change properties of 5% Al<sub>2</sub>O<sub>3</sub>/PAN/PEG after 10, 20, 30, and 50 cycles were investigated by DSC. As can be seen in Figure 5c, the phase change temperatures of 5% Al<sub>2</sub>O<sub>3</sub>/PAN/PEG during heating and cooling remained almost constant over 50 cycles, and the melting and cooling peaks showed good overlap in position and intensity, indicating a stable and reversible phase change behavior of the nanofiber membranes. As can be seen in Figure 5d, the initial melting enthalpy of the nanofiber membranes was 65.12 J·g<sup>−1</sup>, which decreased to 61.05 J·g<sup>−1</sup> after 50 cycles, only about 6.25% lower than the initial value. The enthalpy of crystallization changed from 60.21 J·g<sup>−1</sup> to 57.78 J·g<sup>−1</sup>. These results suggest that a small amount of PEG may have been incompletely encapsulated after 50 cycles and leaked out of the phase change thermoregulation nanofiber membranes when it warmed up to a liquid state, which was lost during multiple accesses to the heating/cooling cycling test, leading to a decrease in the enthalpy of the nanofiber membranes. Together, the nanofiber membranes still had high latent heat after multiple thermal cycling tests. The Al<sub>2</sub>O<sub>3</sub>/PAN/PEG phase change thermoregulated nanofiber membranes have a high energy storage density, suitable phase change temperature, and stable thermal cycling, confirming their potential for PTM applications.

To investigate the effect of Al<sub>2</sub>O<sub>3</sub> on the thermal conductivity of phase change thermoregulated nanofiber membranes, an infrared thermographer connected to a computer was used to record in real time the temperature change of the nanofiber membranes on the thermal bench. The heating stage was first brought up to 50 °C from room temperature, and the temperature rise variations were recorded. When the temperature of all nanofiber membranes stabilized at 50 °C, the heating was turned off, and the cooling variations were recorded. Figure 7a,c shows the thermograms for different Al<sub>2</sub>O<sub>3</sub> concentrations in the nanofiber membranes. All the nanofiber membranes remained at the same ambient temperature (26.3 °C) at 0 s after the heating stage started to heat up. The surface temperatures of the nanofiber membranes were similar after 20 s. However, the 5% Al<sub>2</sub>O<sub>3</sub>/PAN/PEG surface temperature was the lowest (27.3 °C). It is noteworthy that the difference in surface temperature starts to increase after 60 s, with the largest difference at 120 s. The 5% Al<sub>2</sub>O<sub>3</sub>/PAN/PEG (37.6 °C) is significantly lower than the PAN/PEG sample (45.5 °C), indicating that the addition of Al<sub>2</sub>O<sub>3</sub> gives the nanofiber membranes excellent thermal conductivity and thus allows the phase change material to absorb more heat. The 5% Al<sub>2</sub>O<sub>3</sub>/PAN/PEG surface temperature was the lowest compared to the 7% Al<sub>2</sub>O<sub>3</sub>/PAN/PEG (42.4 °C) and 9% Al<sub>2</sub>O<sub>3</sub>/PAN/PEG (39.1 °C), indicating that the thermal

conductivity was optimal and that the 5%  $\text{Al}_2\text{O}_3$  was saturated in the fibers. Similarly, throughout the cooling process, a similar thermal response trend can be observed, with the surface temperature of the 5%  $\text{Al}_2\text{O}_3$ /PAN/PEG sample decreasing relatively slowly. The thermal images illustrate that 5%  $\text{Al}_2\text{O}_3$ /PAN/PEG has the best thermal regulation. To provide a clearer picture of the trend of the nanofiber membranes temperature change, the temperature was recorded every 5 s, resulting in the temperature change curves shown in Figure 7b,d. Compared to the heating stage, the nanofiber membranes exhibited slower temperature changes during the same heating and cooling phases due to the presence of the phase change material PEG, with the 5%  $\text{Al}_2\text{O}_3$ /PAN/PEG always having the smoothest temperature change profile. This is because the phase change material PEG in the  $\text{Al}_2\text{O}_3$ /PAN/PEG undergoes a solid-liquid phase change during heating, which absorbs heat and thus reduces the warming rate of the nanofiber membrane, and a liquid-solid phase change during cooling, which releases heat and thus slows down the cooling rate of the nanofiber membranes. These results show that the  $\text{Al}_2\text{O}_3$ -modified PEG/PAN with a shell layer has a significantly lower temperature change rate compared to the original nanofiber membranes due to the presence of  $\text{Al}_2\text{O}_3$  nanoparticles within the fiber. This demonstrates that the PAN/PEG nanofiber membranes modified with  $\text{Al}_2\text{O}_3$  nanoparticles have thermal storage and temperature regulation properties at this temperature. The best thermoregulation performance was achieved at a concentration of 5%  $\text{Al}_2\text{O}_3$  in the shell layer of the modified nanofiber membranes. The thermal performance of nanofiber membranes can be adversely affected by either increasing or decreasing concentrations.

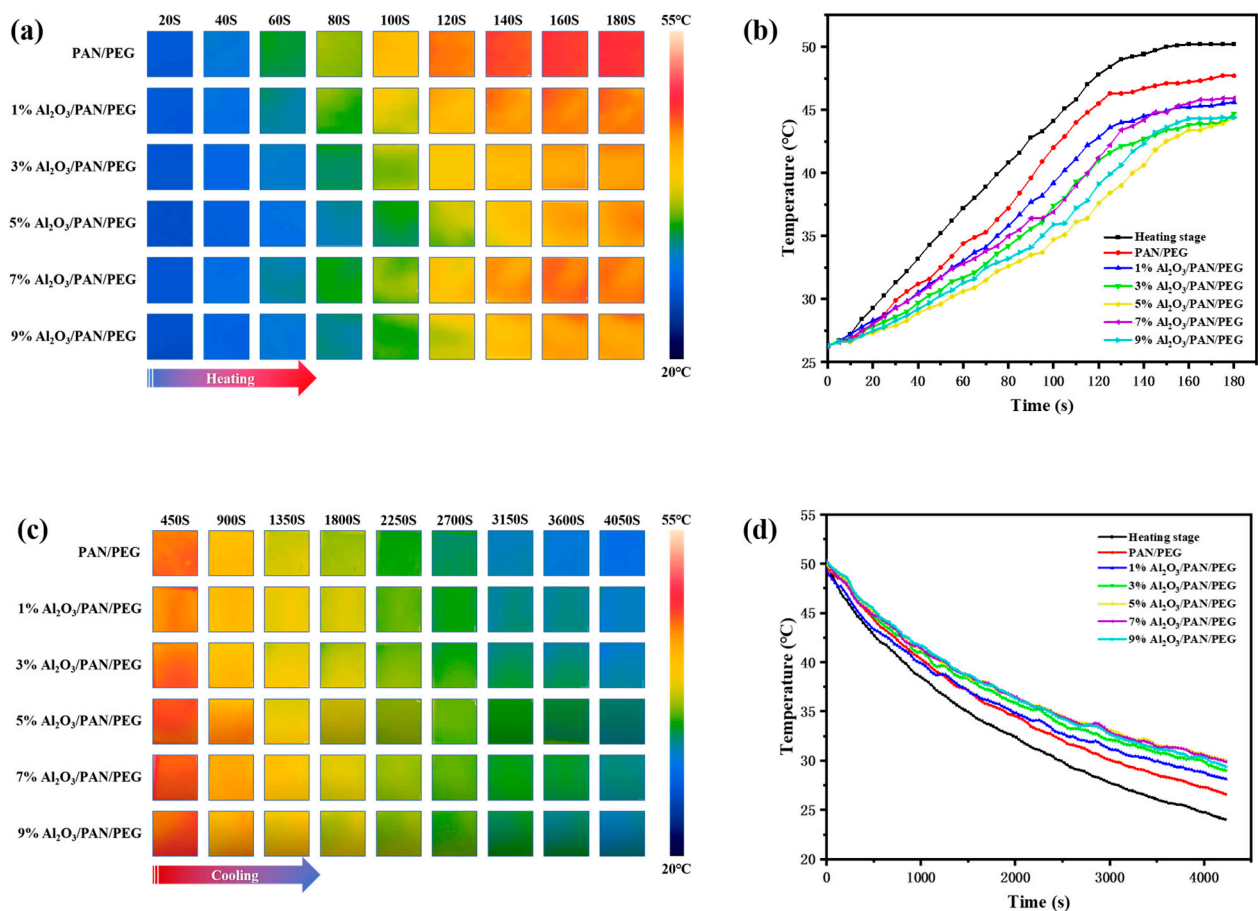


**Figure 7.** Representative thermal images of nanofiber membranes recorded by infrared thermography during (a) heating and (c) cooling process. Temperature evolution plots of the corresponding membranes in the (b) heating and (d) cooling processes.

### 3.5. Analysis of Breathability and Moisture Permeability

The breathability and moisture permeability of the fabric together influences the comfort of human wear [40]. The breathability of different phase change nanofiber membranes was tested according to GB/T 5453, using the evaporation method (positive cup), as shown in Figure 8. The air permeability and moisture permeability curves of the nanofiber membranes showed a similar trend, with an increase in air permeability favoring an increase in moisture permeability. The WVTR of all the membranes was above  $3000 \text{ g}\cdot\text{m}^{-2}\cdot 24 \text{ h}^{-1}$ , with the highest WVTR of  $3723 \text{ g}\cdot\text{m}^{-2}\cdot 24 \text{ h}^{-1}$  at 5%  $\text{Al}_2\text{O}_3$  because both PAN and PEG are hydrophilic materials where the hydrophilic groups help to increase the permeability of water vapor. When the concentration of  $\text{Al}_2\text{O}_3$  is 5%, the fibers in the phase change membrane are the thickest, therefore increasing the gap between the fibers, which is conducive to the passage of water vapor. As  $\text{Al}_2\text{O}_3$  increases, solvent evaporation is incomplete, bonding between fibers occurs, porosity decreases, and, therefore, water vapor permeability decreases. When the concentration of  $\text{Al}_2\text{O}_3$  is 5%, the nanofiber membranes have the best moisture permeability and appropriate breathability, providing a certain degree of comfort for human wear.

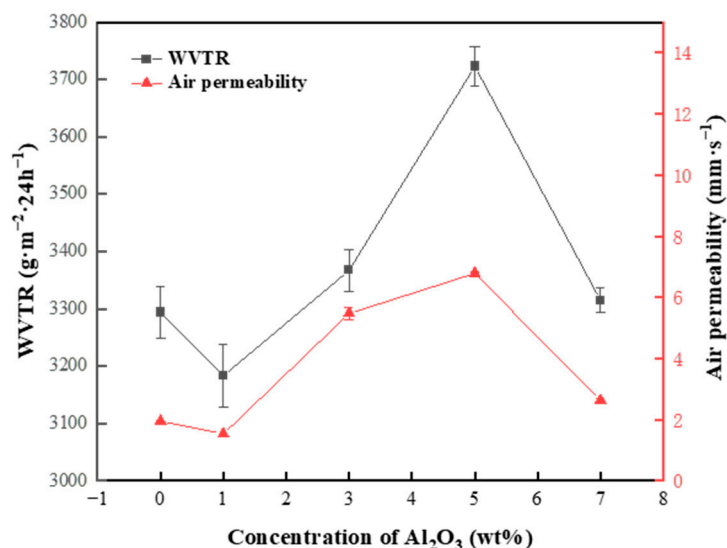


**Figure 8.** Air permeability and moisture permeability of nanofiber membranes with different  $\text{Al}_2\text{O}_3$  concentrations.

## 4. Conclusions

In summary, in this study,  $\text{Al}_2\text{O}_3$ /PAN/PEG phase change thermoregulated nanofiber membranes with a core-shell structure were prepared using a coaxial electrospinning method by adding spherical nano  $\text{Al}_2\text{O}_3$  to the shell layer PAN and increasing the response rate of the core layer phase change material PEG. When the molar fraction ratio of PEG1500 to PEG1000 is 1:9, the phase change temperature of the nanofiber membranes was adjustable between  $33 \text{ }^\circ\text{C}$  and  $38 \text{ }^\circ\text{C}$ , which meets the needs of human comfort. The best overall performance of the resulting nanofiber membranes was achieved at a 5% concentration of added  $\text{Al}_2\text{O}_3$ , with a uniform fiber diameter distribution, a latent heat of melting of  $60.05 \text{ J}\cdot\text{g}^{-1}$ , an onset of phase change temperature of  $31.9 \text{ }^\circ\text{C}$ , and WVTR of  $3723 \text{ g}\cdot\text{m}^{-2}\cdot 24 \text{ h}^{-1}$ , in line with human comfort requirements. During heating, the heating rate of  $\text{Al}_2\text{O}_3$ /PAN/PEG was slower compared to that of the nanofiber membranes without  $\text{Al}_2\text{O}_3$  modification, indicating that the addition of  $\text{Al}_2\text{O}_3$  improved the heat transfer efficiency of the nanofiber membranes. In addition, the nanofiber membranes still had good thermal regulation after 50 cycles of heat and cold. This is due to the effective encapsulation of the core layer of PEG by the coaxial electrospinning technique. The prepared phase change thermoregulation nanofiber membranes have the comprehensive performance of

fast response, reversible phase change, good cycling stability, high moisture permeability, and suitable air permeability, which is expected to be used for PTM textiles.

**Author Contributions:** Conceptualization, L.H. and J.Z.; Methodology, J.Z.; Validation, Y.C. and Z.X.; Formal analysis, Y.C. and Z.X.; Investigation, Y.C., Z.X., C.H., Y.L. and Y.T.; Data curation, Y.C. and Z.X.; Writing—original draft preparation, Y.C., Z.X. and C.H.; Writing—review and editing, J.Z. and Y.T.; Supervision, L.H., and J.Z.; Project administration, L.H.; Funding acquisition, J.Z. All authors have read and agreed to the published version of the manuscript.

**Funding:** This research was funded by the National Natural Science Foundation of China, grant number 51303138.

**Data Availability Statement:** The data are available from the corresponding authors on reasonable request.

**Conflicts of Interest:** The authors declare no conflict of interest.

## References

1. Gugliuzza, A.; Drioli, E. A review on membrane engineering for innovation in wearable fabrics and protective textiles. *J. Membr. Sci.* **2013**, *446*, 350–375. [[CrossRef](#)]
2. Lomax, G.R. Breathable polyurethane membranes for textile and related industries. *J. Mater. Chem.* **2007**, *1727*, 2775–2784. [[CrossRef](#)]
3. Peng, Y.; Cui, Y. Advanced textiles for personal thermal management and energy. *Joule* **2020**, *44*, 724–742. [[CrossRef](#)]
4. Tat, T.; Chen, G.; Zhao, X.; Zhou, Y.; Xu, J.; Chen, J. Smart textiles for healthcare and sustainability. *ACS Nano* **2022**, *169*, 13301–13313. [[CrossRef](#)] [[PubMed](#)]
5. Yang, H.; Liu, Y.; Li, J.; Wang, C.; Li, Y. Full-wood photoluminescent and photothermic materials for thermal energy storage. *Chem. Eng. J.* **2021**, *403*, 126406. [[CrossRef](#)]
6. Hu, R.; Liu, Y.; Shin, S.; Huang, S.; Ren, X.; Shu, W.; Cheng, J.; Tao, G.; Xu, W.; Chen, R.; et al. Emerging materials and strategies for personal thermal management. *Adv. Energy Mater.* **2020**, *17*, 1903921. [[CrossRef](#)]
7. Lan, X.; Wang, Y.; Peng, J.; Si, Y.; Ren, J.; Ding, B.; Li, B. Designing heat transfer pathways for advanced thermoregulatory textiles. *Mater. Today Phys.* **2021**, *17*, 100342. [[CrossRef](#)]
8. Pakdel, E.; Naebe, M.; Sun, L.; Wang, X. Advanced functional fibrous materials for enhanced thermoregulating performance. *ACS Appl. Mater. Interfaces* **2019**, *1114*, 13039–13057. [[CrossRef](#)]
9. Zeng, S.; Pian, S.; Su, M.; Wang, Z.; Wu, M.; Liu, X.; Chen, M.; Xiang, Y.; Wu, J.; Zhang, M.; et al. Hierarchical-morphology metafabric for scalable passive daytime radiative cooling. *Science* **2021**, *373*, 692–696. [[CrossRef](#)]
10. Chen, T.; Fang, Q.; Zhong, Q.; Chen, Y.; Wang, J. Synthesis and thermosensitive behavior of polyacrylamide copolymers and their applications in smart textiles. *Polymers* **2015**, *75*, 909–920. [[CrossRef](#)]
11. Cui, Y.; Gong, H.; Wang, Y.; Li, D.; Bai, H. A thermally insulating textile inspired by polar bear hair. *Adv. Mater.* **2018**, *3014*, 1706807. [[CrossRef](#)]
12. Prajapati, D.G.; Kandasubramanian, B. A review on polymeric-based phase change material for thermo-regulating fabric application. *Polym. Rev.* **2019**, *603*, 389–419. [[CrossRef](#)]
13. Morris, S.J.S. Coupling of interface kinetics and transformation-induced strain during pressure-induced solid–solid phase changes. *J. Mech. Phys. Solids* **2002**, *50*, 1363–1395. [[CrossRef](#)]
14. Guo, Z.; Sun, C.; Wang, J.; Cai, Z.; Ge, F. High-performance laminated fabric with enhanced photothermal conversion and joule heating effect for personal thermal management. *ACS Appl. Mater. Interfaces* **2021**, *137*, 8851–8862. [[CrossRef](#)] [[PubMed](#)]
15. Liu, X.; Jin, X.; Li, L.; Wang, J.; Yang, Y.; Cao, Y.; Wang, W. Air-permeable, multifunctional, dual-energy-driven MXene-decorated polymeric textile-based wearable heaters with exceptional electrothermal and photothermal conversion performance. *J. Mater. Chem. A* **2020**, *825*, 12526–12537. [[CrossRef](#)]
16. Wu, H.; Zhao, L.; Si, Y.; Zhang, S.; Yu, J.; Ding, B. Ultralight and superelastic fibrous sponges with effective heat preservation and photo-thermal conversion for personal cold protection. *Compos. Commun.* **2021**, *25*, 100766. [[CrossRef](#)]
17. Yuan, K.; Shi, J.; Aftab, W.; Qin, M.; Usman, A.; Zhou, F.; Lv, Y.; Gao, S.; Zou, R. Engineering the thermal conductivity of functional phase-change materials for heat energy conversion, storage, and utilization. *Adv. Funct. Mater.* **2019**, *308*, 1904228. [[CrossRef](#)]
18. Lu, Y.; Xiao, X.; Fu, J.; Huan, C.; Qi, S.; Zhan, Y.; Zhu, Y.; Xu, G. Novel smart textile with phase change materials encapsulated core-sheath structure fabricated by coaxial electrospinning. *Chem. Eng. J.* **2019**, *355*, 532–539. [[CrossRef](#)]
19. Chen, Y.; Zhang, Q.; Wen, X.; Yin, H.; Liu, J. A novel CNT encapsulated phase change material with enhanced thermal conductivity and photo-thermal conversion performance. *Sol. Energy Mater. Sol. Cells* **2018**, *184*, 82–90. [[CrossRef](#)]
20. Iqbal, K.; Sun, D. Development of thermo-regulating polypropylene fibre containing microencapsulated phase change materials. *Renew. Energy* **2014**, *71*, 473–479. [[CrossRef](#)]
21. Rabha, D.K.; Muthukumar, P. Performance studies on a forced convection solar dryer integrated with a paraffin wax-based latent heat storage system. *Sol. Energy* **2017**, *149*, 214–226. [[CrossRef](#)]



22. Du, Y.; Huang, H.; Hu, X.; Liu, S.; Sheng, X.; Li, X.; Lu, X.; Qu, J. Melamine foam/polyethylene glycol composite phase change material synergistically modified by polydopamine/MXene with enhanced solar-to-thermal conversion. *Renew. Energy* **2021**, *171*, 1–10. [[CrossRef](#)]
23. Griffiths, K.; Halcovitch, N.R.; Griffin, J.M. Long-Term Solar Energy Storage under Ambient Conditions in a MOF-Based Solid–Solid Phase-Change Material. *Chem. Mater.* **2020**, *32*, 9925–9936. [[CrossRef](#)]
24. Aftab, W.; Huang, X.; Wu, W.; Liang, Z.; Mahmood, A.; Zou, R. Nanoconfined phase change materials for thermal energy applications. *Energy Environ. Sci.* **2018**, *11*, 1392–1424. [[CrossRef](#)]
25. Chen, X.; Gao, H.; Yang, M.; Xing, L.; Dong, W.; Li, A.; Zheng, H.; Wang, G. Smart integration of carbon quantum dots in metal-organic frameworks for fluorescence-functionalized phase change materials. *Energy Storage Mater.* **2019**, *18*, 349–355. [[CrossRef](#)]
26. Yang, H.; Chao, W.; Di, X.; Yang, Z.; Yang, T.; Yu, Q.; Liu, F.; Li, J.; Li, G.; Wang, C. Multifunctional wood based composite phase change materials for magnetic-thermal and solar-thermal energy conversion and storage. *Energy Convers. Manag.* **2019**, *200*, 112029. [[CrossRef](#)]
27. Liu, C.; Rao, Z.; Zhao, J.; Huo, Y.; Li, Y. Review on nanoencapsulated phase change materials: Preparation, characterization and heat transfer enhancement. *Nano Energy* **2015**, *13*, 814–826. [[CrossRef](#)]
28. Lu, Y.; Xiao, X.; Zhan, Y.; Huan, C.; Qi, S.; Cheng, H.; Xu, G. Core-Sheath Paraffin-Wax-Loaded Nanofibers by Electrospinning for Heat Storage. *ACS Appl. Mater. Interfaces* **2018**, *10*, 12759–12767. [[CrossRef](#)]
29. Niu, Z.; Yuan, W. Smart nanocomposite nonwoven wearable fabrics embedding phase change materials for highly efficient energy conversion-storage and use as a stretchable conductor. *ACS Appl. Mater. Interfaces* **2021**, *13*, 4508–4518. [[CrossRef](#)]
30. Chen, C.; Zhao, Y.; Liu, W. Electrospun polyethylene glycol/cellulose acetate phase change fibers with core–sheath structure for thermal energy storage. *Renew. Energy* **2013**, *60*, 222–225. [[CrossRef](#)]
31. Sun, S.-X.; Xie, R.; Wang, X.-X.; Wen, G.-Q.; Liu, Z.; Wang, W.; Ju, X.-J.; Chu, L.-Y. Fabrication of nanofibers with phase-change core and hydrophobic shell, via coaxial electrospinning using nontoxic solvent. *J. Mater. Sci.* **2015**, *50*, 5729–5738. [[CrossRef](#)]
32. Lan, T.; Shao, Z.-q.; Wang, J.-q.; Gu, M.-j. Fabrication of hydroxyapatite nanoparticles decorated cellulose triacetate nanofibers for protein adsorption by coaxial electrospinning. *Chem. Eng. J.* **2015**, *260*, 818–825. [[CrossRef](#)]
33. Wu, Y.; Chen, C.; Jia, Y.; Wu, J.; Huang, Y.; Wang, L. Review on electrospun ultrafine phase change fibers (PCFs) for thermal energy storage. *Appl. Energy* **2018**, *210*, 167–181. [[CrossRef](#)]
34. Yu, D.G.; Li, J.J.; Zhang, M.; Williams, G.R. High-quality janus nanofibers prepared using three-fluid electrospinning. *Chem. Commun.* **2017**, *53*, 4542–4545. [[CrossRef](#)]
35. Qi, G.-Q.; Yang, J.; Bao, R.-Y.; Liu, Z.-Y.; Yang, W.; Xie, B.-H.; Yang, M.-B. Enhanced comprehensive performance of polyethylene glycol based phase change material with hybrid graphene nanomaterials for thermal energy storage. *Carbon* **2015**, *88*, 196–205. [[CrossRef](#)]
36. Cabeza, L.F.; Castell, A.; Barreneche, C.; de Gracia, A.; Fernández, A.I. Materials used as PCM in thermal energy storage in buildings: A review. *Renew. Sustain. Energy Rev.* **2011**, *15*, 1675–1695. [[CrossRef](#)]
37. Ng, D.-Q.; Tseng, Y.-L.; Shih, Y.-F.; Lian, H.-Y.; Yu, Y.-H. Synthesis of novel phase change material microcapsule and its application. *Polymer* **2017**, *133*, 250–262. [[CrossRef](#)]
38. Miguel, S.P.; Ribeiro, M.P.; Coutinho, P.; Correia, I.J. Electrospun polycaprolactone/aloe vera\_chitosan nanofibrous asymmetric membranes aimed for wound healing applications. *Polymers* **2017**, *9*, 183. [[CrossRef](#)]
39. Xue, J.; Wu, T.; Dai, Y.; Xia, Y. Electrospinning and electrospun nanofibers: Methods, materials, and applications. *Chem. Rev.* **2019**, *119*, 5298–5415. [[CrossRef](#)]
40. Shen, B.; Zhang, D.; Wei, Y.; Zhao, Z.; Ma, X.; Zhao, X.; Wang, S.; Yang, W. Preparation of Ag doped keratin/PA6 nanofiber membrane with enhanced air filtration and antimicrobial properties. *Polymers* **2019**, *11*, 1511. [[CrossRef](#)]

**Disclaimer/Publisher’s Note:** The statements, opinions and data contained in all publications are solely those of the individual author(s) and contributor(s) and not of MDPI and/or the editor(s). MDPI and/or the editor(s) disclaim responsibility for any injury to people or property resulting from any ideas, methods, instructions or products referred to in the content.